



Research Paper

Characteristics of elemental carbon overlayers over hematite electrodes prepared by electrodeposition with organic acid additives



Tsing Hai Wang^{a,*}, Chia-Che Chiang^a, Yi-Lin Wu^a, Cheng Lin^a, Yu-Jung Cheng^a,
Yi-Kong Hsieh^a, Chu-Fang Wang^{a,*}, C.P. Huang^b

^a Biomedical Engineering and Environment Sciences, National Tsing Hua University, Hsinchu, Taiwan

^b Department of Civil & Environmental Engineering, University of Delaware, Newark, DE, USA

ARTICLE INFO

Article history:

Received 8 July 2016

Received in revised form 11 January 2017

Accepted 2 February 2017

Available online 3 February 2017

Keywords:

Hematite

Carbon overlayer

Photoelectrochemical cell

Electrodeposition

Chelation

ABSTRACT

We report that inducing elemental carbon overlayers on hematite electrodes is a universal case that can be achieved by electrodeposition with addition of a wide range of organic acid following by thermal treatment. The thickness of elemental carbon overlayers directly affects the photocurrent density of as-obtained samples, which can be adjusted by selection of organic acid and electrodeposition pH. An optimal carbon overlayer of approximately 2–5 nm enhanced a 10 times higher photocurrent density (2.0 mA/cm² at 0.4 V_{SCE}) in comparison with those without carbon overlayers. While carbon overlayers were effective in passivating surface states, a capacitor was formed at the hematite/carbon overlayer interface upon illumination for 90 min. Our results clearly demonstrated the characteristics of effective carbon overlayers include (i) passivating surface states to reduce the onset photocurrent potential, (ii) injecting additional charges to enhance the photocurrent plateau, and (iii) the durability to sustain a long period of sunlight illumination.

© 2017 Published by Elsevier B.V.

1. Introduction

Sunlight harvesting is one of the most promising alternatives in curtailing globe warming through the use of low carbon footprint energy such as hydrogen by photoelectrochemical (PEC) water splitting. To this end, semiconductor catalysts are the key components necessary for harvesting sunlight through the generation, separation, and transport of charge carriers at semiconductor/aqueous interfaces. Among all photocatalysts, material abundance, chemical stability over a wide pH range, and narrow band gap structure enabling the efficient utilization of a significant portion of visible light make hematite an attractive material selection. Several methods have been proposed to prepare hematite electrode for PEC applications [1]. Among all of these methods, electrodeposition has received the most attention due to its simplicity, particularly for large scale manufacturing [2]. For instance, granular and compact nanocrystalline hematite electrodes prepared by pulse reverse electrodeposition method has exhibited a photocurrent density of 0.5 mA/cm² at 1.23 V vs. RHE [3]. Zeng et al. reported

that a hematite electrode could generate a photocurrent density of 1.35 mA/cm² at 1.23 V vs. RHE by controlling the thickness and crystallinity of the electrode carefully by electrodeposition time and annealing conditions [4]. The variations in the crystallographic properties will enhance hole transport and collection and bring about high current intensity [5]. Furthermore, Zandi et al. reported that cobalt-phosphate (Co-Pi) cocatalysts greatly enhanced the photocurrent density by 70% over electrodeposited dendritic type hematite electrodes due to increase in the suppression of the photogenerated electron–hole recombination [6]. Chemelewski et al. reported photocurrent density of 10 mA/cm² by doping oxygen evolution reaction (OER) catalysts with metals, such as Ni-doped goethite (Ni:FeOOH) via electrodeposition [7]. Passivating surface trapping states with a thin layer of Al₂O₃, In₂O₃ or Ga₂O₃ was also reported to greatly enhance photocatalytic performance [8]. Passivation layers could effectively improve the charge-separation and charge-transfer processes across semiconductor–liquid interfaces as evidenced by significant changes in surface capacitance and radiative recombination [8]. One of the most important characteristics of passivation overlayers is the cathodic (negative) shift of the overpotential due to suppression of the electron–hole recombination, which increases the photovoltage and band bending [9]. Recently, a thin elemental carbon overlayer has been successfully synthesized by pyrolysis of ferrocene over hematite using crucible

* Corresponding authors.

E-mail addresses: thwang@mx.nthu.edu.tw (T.H. Wang), cfwang@mx.nthu.edu.tw (C.-F. Wang).

which center region was less accessible to atmospheric oxygen and therefore carbon overlayers were formed readily during sintering. Results of X-ray absorption spectroscopy analyses revealed that a significant amount of oxygen vacancy was concurrently introduced by the carbon overlayers [10]. We have also discovered that the addition of citric acid to the electrolyte will form elemental carbon overlayers on the electrodeposited hematite electrodes that yielded a photocurrent density of around 2.1 mA/cm^2 at 0.4 V versus SCE under standard illumination [11]. Although organic acids are frequently added in electrolyte to stabilize metal ions, induced carbon overlayers have been discussed in the literature. Importantly, the PEC performance was closely related to the thickness of surface carbon layer [11]. We have speculated that the enhanced PEC performance is due to the passivation effect that reduces the hole-electron recombination loss at surface states. Despite a lack of understanding the functionality of the carbon overlayer, it is clear that the elemental carbon overlayer will greatly enhance the photocatalytic activity of hematite electrodes. Two important questions arise: first, is citric acid the only organic additive capable of creating carbon overlayers?; second, what are the typical characteristics of carbon overlayer effectively enhancing PEC activity and how to characterize them?

In order to answer the above questions, a series of hematite electrodes were prepared by electrodeposition in electrolyte containing 0.1 M of five different organic acids, namely, acetate (Ace), citrate (Cit), EDTA, salicylate (Sal), and ascorbate (Asc) as a function of pH. Based on MINEQL software [12], the formation constants ($\log K$) are 9.59, 13.10, 29.20, 29.30, and 11.57, for the Fe(III) complexes of Ace, Cit, EDTA, Sal, and Asc [13], respectively. The organic acids selected have a wide range of affinity toward Fe^{3+} , which will affect their adsorption onto iron oxyhydroxide (FeOOH) at different pH and the subsequent formation of carbon layers. Therefore it will address the first question of the specificity of the formation of carbon overlayers. That is, is citric acid the only organic acid forming carbon overlayers? Then, the characteristics for an effective carbon overlayer were investigated and suggested for the perspective of manufacturing high photocatalytic hematite electrodes in the future.

2. Experimental section

2.1. Preparation of $\alpha\text{-Fe}_2\text{O}_3$ photoelectrodes via electrodeposition

All chemicals used in this study were of ACS grade purchased from Sigma-Aldrich and Merck and used as-received without any further purification. To prepare electrodeposited $\alpha\text{-Fe}_2\text{O}_3$ electrodes, FTO glass substrates ($2 \times 1 \text{ cm}$, working electrode) were immersed in an electrodeposition bath with a Pt plate ($1 \times 1 \text{ cm}$) as a counter electrode and a saturated calomel electrode (SCE) as a reference. The electrolyte was consisted of 0.1 M of iron(III) chloride hexahydrate and 1.0 M of sodium nitrate with/without 0.1 M citric acid additives in different pH values. The electrodeposition was conducted in chronopotentiometry mode (at 50 mA for 5 min , CH Instrument, CHI 608E). At the end of electrodeposition, the samples were first gently rinsed with deionized water and then air-dried followed by a two-step heating treatment (500°C for 1 h then 750°C for 10 min) at a heating rate of $10^\circ\text{C}/\text{min}$ in air. Six samples were prepared for each condition and the one exhibited the photocurrent density closest to the average value (the relative standard deviation, RSD, about 15%) was chosen for further characterization.

2.2. PEC measurements

For PEC measurements, hematite electrodes were covered by a stripe of nonconductive Teflon by leaving a working area ($1 \times 1 \text{ cm}$)

for exposing to simulated sunlight (AM 1.5 G with the light power density of 100 mW/cm^2). All PEC measurements were conducted using a CHI 608E electrochemical workstation in a three-electrode configuration as mentioned above in an electrolyte containing 1.0 M of NaOH (pH 13.6). The measured potential was swept from -0.5 V to 1.0 V vs. SCE at a scan rate of 50 mV/s . To determine the charge carrier density of the hematite samples, Mott–Schottky (MS) plots were derived from the electrochemical impedance obtained in the potential between -0.5 – 0.7 V vs. SCE at a frequency of 10 kHz in dark and the capacitance was extracted according to Eq. (1) [11]:

$$Z'' = 1/2\pi fC \quad (1)$$

where the Z'' stands for the imaginary impedance, f is the scan frequency and C refers to the capacitance of the sample measured. Note that the validity of using only one frequency point to extract capacitance for MS plots is built on the following assumption: two capacitances are to be considered, namely, the space charge region and the double layer, respectively. Since the space charge capacitance is much smaller than that of the double layer (by 2–3 orders of magnitude) and they are in series, the contribution of the double layer capacitance to the total capacitance is negligible due to that the total capacitance is the sum of their reciprocals. This means the capacitance value calculated from this model is assumed to be the value of the space charge capacitance (capacitance of hematite bulk in this study) and therefore a high frequency on the order of kHz is required. Electrochemical impedance spectroscopy (EIS) measurement was carried out under illumination with $+0.1 \text{ V}$ applied voltage by the same workstation in the frequency range of 1 Hz – 100 kHz . Obtained data were fitted by an equivalent circuit using the Zview software.

2.3. Characterization of electrode

The scanning electron microscopy (SEM) images of hematite nanostructures were obtained using JSM700F, JEOL scanning electron microscope with acceleration voltage of 20 kV . High-Resolution transmission electron microscopy (HRTEM) images and energy dispersive X-ray analysis (EDX) were recorded using JEOL JEM-2100 HRTEM. To prepare HRTEM specimens, electrodeposited hematite samples were scratched from the surface of FTO substrates into 5 mL deionized water using a razor blade. After 10 min of sonication, the suspensions were transferred onto a holey carbon thin film supported by a copper grid. X-Ray Diffractometer (XRD, D2 Phaser diffractometer, Brucker) and X-ray photoelectron Spectrometer (XPS, PHI Quantera SXM/Auger) were utilized for the structure and the oxidation state characterization. Batch adsorption experiments were performed by dispersing 1.0 g FeOOH (Sigma-Aldrich) in 100 mL solution containing 10 mg/L of studied organic species with 10 mM of NaCl as the background electrolyte. The pH adjustment was conducted using either 0.1 N HCl or NaOH . In the end of 24 h reaction under vigorously stirring, the equilibrated pH was recorded and 1.0 mL mixture was collected and filtrated using a $0.25 \mu\text{m}$ PTFE filter. The concentration of organic acid remaining in the solution was determined using total organic carbon analyzer (Aurora 1030WOI Analytical TOC analyzer) and the difference in the concentration is assumed the amount of organic acid adsorbed on FeOOH particles.

3. Results and discussions

Fig. S1 shows typical J-V curves of hematite electrodes electrodeposited with 0.1 M of ascorbic acid additives at different pH values. Observed photocurrent density at $0.4 \text{ V}_{\text{SCE}}$ was recorded and arranged in Fig. 1a. As shown in Fig. 1a, it is noted that the photocurrent density of the different hematite electrodes was sensitive

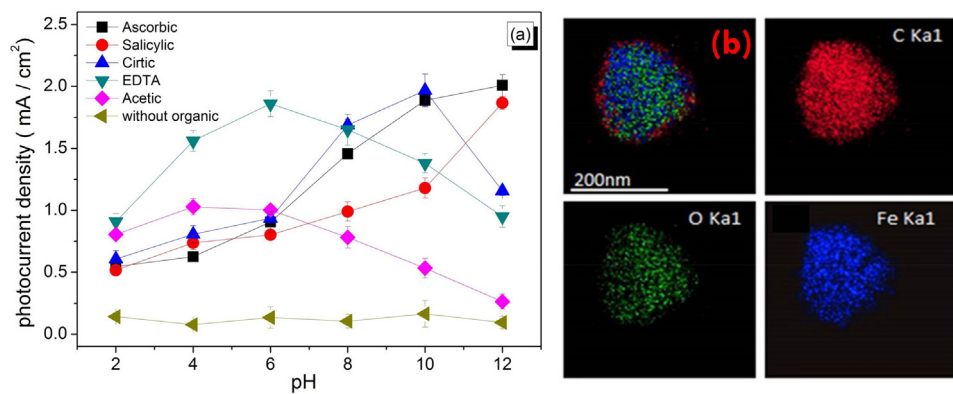


Fig. 1. (a) Photocatalytic performance of electrodeposited hematite electrodes as a function of electrodeposition pH. (b) Typical HRTEM mapping images of electrodeposited hematite particles in the presence of citrate at pH 8. Samples were collected by sonicating as-obtained hematite electrodes in deionized water for 10 min.

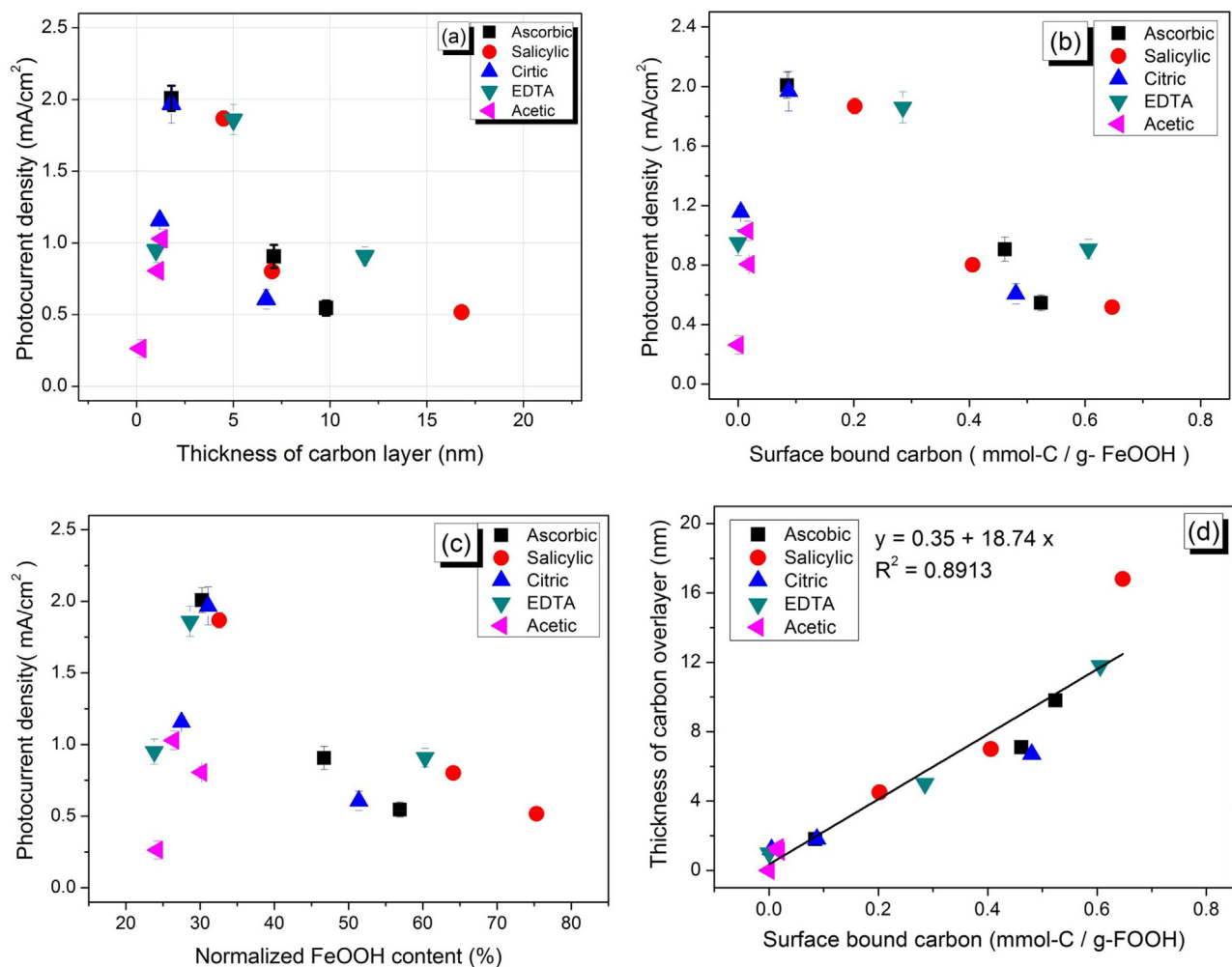


Fig. 2. Relationship between photocurrent density measured at +0.4 V vs SCE and (a) the thickness of carbon overlayers, (b) the amount of surface bound carbon determined from adsorption experiments, (c) the normalized FeOOH content determined from XPS analyses, and (d) relationship between the amount of surface bound carbon and the thickness of carbon overlayer. The amount of surface bound carbon was determined by the amount of adsorbed organic acid multiplying with its carbon moiety; for example, multiplying 10 for adsorbed EDTA as one mole of EDTA has 10 mol of carbon in its structure.

to the electrodeposition pH. Consistent with our previous observations [11], all electrodes exhibited photocurrent density higher than that prepared without organic acid additives (~0.3 mA/cm²). HRTEM images (Fig. S2) and mapping images (Fig. 1b) further suggested that carbon overlayers were closely related to the enhanced photocurrent density. The source of carbon overlayer was surface

bound organic acids in micropores of hematite film as no carbon overlayer was found in hematite particles collected in the end of adsorption experiments (after thermal treatment) (Figs. 2b and Fig. S3). Specifically, the electrodeposited hematite films were essentially agglomerations of FeOOH nanoparticles and surface bound organic acids in micropores made up of coherently stacked FeOOH

nanoparticles were less accessible to ambient oxygen during sintering. As a result, a carbon overlayer was formed and significantly affected the photocatalytic performance of hematite electrodes. Interestingly, an optimal thickness of around 2–5 nm exhibited the highest photocatalytic activity among all hematite electrodes studied (Fig. 2a). Clearly, our results answer the first question convincingly that carbon overlayers can be formed by a wide variety of organic acid additives that citric acid is not the exclusive reagent. Our results have provided a new strategy to manufacturing high performance hematite electrodes, simply by adding organic acid in the electrolyte during electrodeposition. The thickness of carbon overlayers can be controlled by the type of organic acid and electrodeposition pH, which governs the affinity of organic acids toward iron oxyhydroxide as evidenced by separate adsorption experiments (Figs. 2b and S3).

It is then to answer the second question of what unique characteristics make carbon overlayers effective in promoting photoactivity. Three typical hematite electrodes with thin, thick, and without carbon overlayers, respectively, were selected for further investigations. As shown in Fig. S4a, the intense C1s XPS peaks clearly indicated the presence of carbon overlayers while the Fe 2p XPS spectra, the Fe 2p3/2 peak at 710.9 eV and Fe 2p1/2 peak at 724.0 eV, identified the nature of hematite (Fig. S4b). The deconvoluted C1s XPS peak based on the NIST X-ray Photoelectron Spectroscopy Database [14], furthermore suggested that the sample with a thin carbon overlayer contained high fraction of elemental carbon (at 284.3–284.5 eV) along with a small fraction of carboxyls at 288.2 eV (Fig. S4c). A close inspection of O 1s XPS spectra revealed that the hematite electrode with a thick carbon overlayer had a high fraction of iron hydroxyl groups, likely resulted from the FeOOH phase (Fig. S4d). Note that deconvolution of O1s spectra would not be the best means of identifying phases of iron oxide, as the presence of surface hydroxyls does not necessarily indicate the presence of the FeOOH phase. The high-energy peak may also be associated with carbonates, adsorbed water or even nitrates even though the XPS analyses were conducted under ultrahigh vacuum ($<5 \times 10^{-10}$ Torr). It is a practical alternative, however, as the non-Gaussian-like Fe peak of Fe-bearing phases makes the deconvolution rather challenging. For an approximation, we adopted the term FeOOH in the content to account for all low crystallized surface iron oxide phases. The above results address the characteristics issue of an effective carbon overlayer, that is, low crystalline iron oxide phases on the hematite surface. It has been reported that rapid and high temperature treatment (800 °C) can effectively enhance the PEC performance of hematite electrodes by removing the low crystallized surface iron oxide phases [15]. Two surface states have been identified: one is the reduced surface species, which is the H₂O oxidation intermediates appearing at the potential at around the onset photocurrent potential [16] and the other is the oxygen p-hybridized states located just below the conduction band minimum [17]. We therefore arrange Fig. 2a to explore the connections among surface bound organic acid, low crystallized surface iron oxide phases and photocatalytic performance.

By plotting the photocurrent density against the amount of surface bound carbon determined from separate adsorption experiments, it is noted that the maxima photocurrent density occurred at approximately 0.1–0.3 mmol bound carbon per gram of FeOOH (Fig. 2b). This amount of surface bound carbon led to 30% of the normalized FeOOH content (FeOOH content over total Fe content) obtained from XPS analyses (Fig. 2c). Excessive bound organic acids will lead to an increase in the fraction of low crystallized hematite. Furthermore, the thickness of carbon overlayers was proportional to the amount of surface bound carbon (Fig. 2d). This clearly indicated that the surface bound organic acid, low crystallized surface iron oxide phases and photocatalytic performance

are closely interdependent. We hypothesized that the interaction between organic acid and iron oxyhydroxides will hinder phase transformation during sintering. Accordingly, increase in FeOOH content is noted accompanied with increasing bound surface carbon and thick carbon overlayers (Fig. 2d). Nevertheless, it is certain that carbon overlayers are obviously capable of enhancing photocatalytic performance of hematite electrodes (Fig. 1). Importantly, Yu, et al. demonstrated that hematite electrodes modified with nanostructured FeOOH exhibited cathodic shift of onset potential by 0.14 V and four-times higher photocurrent density [18]. This finding strongly suggests that low crystallized iron oxides is not necessary the surface states responsible for deteriorating the photocatalytic performance. Our results show that a fraction of 30% of surface low crystallized iron oxides yields the optimal photocatalytic performance. Accordingly, a *a priori* requirement for an effective carbon overlayer is to regulate the degree of surface low crystallized iron oxide phases.

It is generally believed that passivating surface states through suppressing recombination loss reduces the photocurrent onset potential while increased photocurrent plateau is mainly controlled by the conductivity of hematite and band bending [19]. As shown in Fig. 3a, both thin and thick carbon overlayers cathodically shifted the photocurrent onset potential by 0.1 V to *ca.* -0.27 V_{SCE} (0.777 V_{RHE}, based on $V_{RHE} = V_{SCE} + 0.24 + 0.059 \text{ pH}$) [20] versus -0.17 V_{SCE} of no carbon overlayers. Similar cathodic shift in onset potential has been reported by using catalysts such as NiFeOx [21], high temperature treatment [14] and constructing heterojunction configurations [22] in hematite electrodes. While passivation effect is likely to account for lower onset potential, it is uncertain if enhanced photocurrent plateau is also resulted from the improved conductivity and band bending by doping effect. To answer this concern, MS plots were arranged (Fig. 3b) and showed that the charge carrier density for hematite electrodes of no, thin, and thick carbon overlayers were $2.53, 9.72$ and $17.7 \times 10^{12} \text{ cm}^{-3}$, respectively. This indicated that in addition to the passivation effect that suppressed recombination loss [18], increase in charge carrier density was also responsible for enhanced photocurrent plateau. Although the connection between enhanced charge carrier density and surface FeOOH content remains unclear (as lattice Fe²⁺ will inject additional intrinsic defects of oxygen vacancy), apparently the second characteristics of effective carbon overlayers will be to simultaneously introduce additional charge carriers to hematite electrodes. Deng et al. reported similar charge carrier density enhancement in hematite electrodes prepared by the pyrolysis of ferrocene and that the modified electronic structure due to surface carbon coating layers also was also responsible for high photocurrent density [10]. To explore the influence of carbon overlayers on electronic property of hematite, impedance spectra were recorded under illumination and fitted with the surface state equivalent circuit (Fig. S5) [16,19]. As shown in Fig. 3c, the hematite electrode without carbon overlayers had a broadened peak of capacitance of the surface states, C_{trap}, at 0.1 V vs SCE. By contrast, a shift in C_{trap} maxima to *ca.* -0.2 V_{SCE} and no significant C_{trap} peak were concurrently noted in samples with thin and thick carbon overlayers. Despite no C_{trap} peaks identified in the latter two electrodes, it is interesting to note that as long as half of the surface states are emptied (passivated) a cathodic shift in onset of photocurrent will occur. Further, a thick carbon overlayer passivates surface state was more effectively than a thin one as evidenced by much lower C_{trap} values noted in the entire potential range studied. The charge transfer resistance (R_{ct,trap}, Fig. 3d) of hematite with thin and thick carbon overlayer are 30% and 10% that of electrodes without carbon overlayers, respectively. This again suggests that carbon overlayer can effectively passivate surface states. Importantly, carbon overlayer likely will also indirectly enhance the band bending effect by reducing the Fermi level pinning effect at the Helmholtz layer [21].

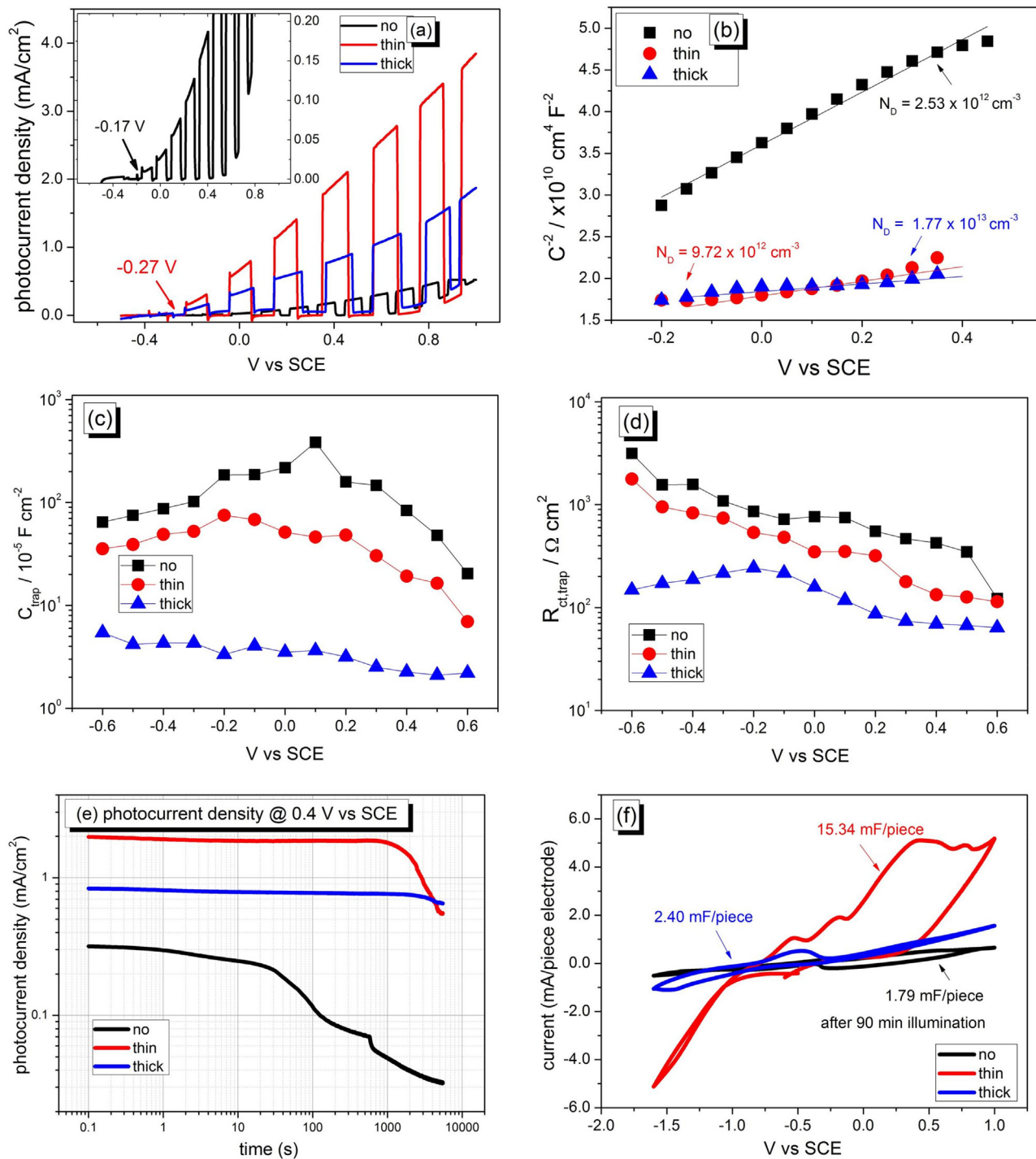


Fig. 3. Characteristics of hematite electrodes without (black) and with thin (red) and thick (blue) carbon overlayer. Shown are (a) light chopping experiments, (b) Mott-Schottky plots of samples from (a) measured in the dark, derived charge carrier density (N_D) was included (c) C_{trap} versus applied potential, (d) charge transfer resistance from surface states, $R_{\text{ct,trap}}$, versus applied potential, (e) photocurrent-time curve under illumination, and (f) the CV curves in the end of 90 min of illumination. (For interpretation of the references to colour in this figure legend, the reader is referred to the web version of this article.)

and extending the space charge region [19] through the suppression of surface states. However, decoupling the interplay between passivation and band bending effect is rather difficult and it is not within the scope of this present study.

In addition to passivating surface states and doping extra charges by carbon overlayers, their chemical stability is another important criterion for the perspective of large scale application in the future. As shown in Fig. 3e, the photocurrent density of hematite electrodes without carbon overlayers dramatically deteriorated

after 30 s of illumination whereas the presence of carbon overlayers allowed photocurrent density to sustain for over 1000 s. The cause of photocurrent degradation is complicated and is beyond the scope of the present study. However, it is clear that a capacitor, likely resulting from either surface redox couple or surface double layer charging capacity [21,23], was formed at the hematite/carbon overlayer interface upon illumination for 90 min, which is extremely remarkable for a thin carbon overlayer. It has been reported that Ga_2O_3 [24] and FeOOH [18] overlayers could effectively sustain

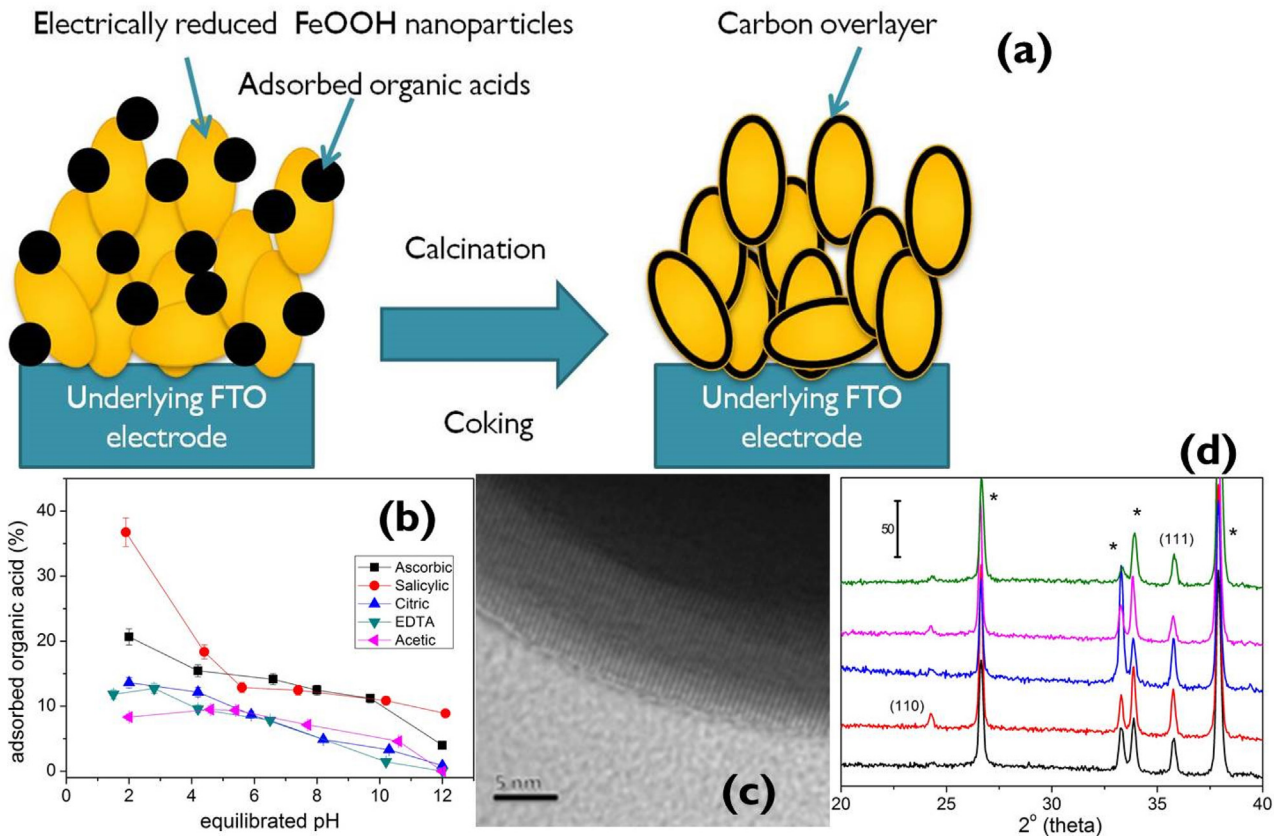


Fig. 4. (a) Proposed mechanism accounting for the formation of elemental carbon overlayer. Adsorbed organic acids in the pores resulting from the stacking of electrically reduced FeOOH nanoparticles have less access of ambient oxygen and thus adsorbed organic acids are converted to elemental carbon overlayer in the following calcination through coking process; (b) results of batch experiments of organic adsorption to FeOOH; (c) HRTEM image of hematite particles collected by sonicating electrode prepared in an electrodeposition condition with 0.1 M EDTA at pH 2; (d) representative XRD patterns of hematite electrodes electrodeposited in the condition with 0.1 M citric acid at pH 2, 4, 6, 8, 10, respectively from bottom to up. The * refers to the diffraction from FTO substrates while the indexed of hematite was conducted using database of JCPDS 33-0664. Inserted scale bar stands for an intensity of 50 cps.

photocurrent for over 24 and 70 h, respectively. Improving the durability of carbon overlayers would be an interesting research topic in the future. We admit that the morphology effect on photocatalytic performance enhancement is not excluded as no specific patterns can be concluded based on SEM images (Fig. S6). Evolution on the morphology of hematite nanoparticles during electrodeposition is realized as a result of the dynamic adsorption and desorption of organic acids on the electroreduced iron oxyhydroxides. The mode and dynamics of interfacial interactions between the organic acid and the iron oxyhydroxide will eventually affect the orientation of hematite. The correlation between the affinity of organic acid toward iron oxyhydroxides and subsequent PEC performance is important to understanding the functionality of carbon overlayers and ongoing research topic in our group.

Based on our results, it is concluded that carbon overlayer can effectively enhance photocurrent through passivating surface states. However, involved mechanism regarding how carbon overlayers were formed, why the photocurrent density of the different hematite electrodes was sensitive to the electrodeposition pH and what is the connection between the characteristics of carbon overlayer as well as the surface morphologies of hematite and photocatalysis performance remain unclear. Based on observations from five studied organic acids herein, the most presumably explanation accounting for these behaviors might be related to the adsorption characteristics of the additives. In an electrodeposition system, Fe(III) ions accept electrons and then electrically reduced and stabilized by organic acid and water molecules [2]. Dehydration of reduced species will simultaneously accompany with the ther-

modynamically favorable oxidation of Fe(II) to Fe(II) (the standard potential of $\text{Fe}(\text{III}) + \text{e}^- \rightarrow \text{Fe}(\text{II})$ is $+0.77\text{ V}$) [25], leading to the deposition of insoluble FeOOH nanoparticles on the FTO substrate [2]. This means the porous structure of electrodeposited FeOOH electrode is actually resulting from the stack of electrically reduced FeOOH nanoparticles [21]. In this circumstance, surface adsorbed organic acids retaining in the pores (specifically speaking, voids) of stacked FeOOH nanoparticles would have less access to ambient oxygen in the following calcination process and therefore become the source of carbon overlayers (Fig. 4a). As adsorption of organic acids to FeOOH is strongly pH-dependent (Fig. 4b), it suggests electrostatic interaction plays an important role in the adsorption. This explains the observations that higher adsorption is noted in acidic environment than in the alkaline environment. As adsorbed organic acids function as the precursor of carbon overlayer, a general pattern that the thickness of carbon overlayer decreases with increasing pH is therefore observed (Fig. S2). This also explains the trend that the thickness of carbon overlayer is linearly proportional to the content of adsorbed carbon (Fig. 2d). In addition to electrostatic interaction, enhanced adsorption of salicylic acid in acidic environment is noted, which was suggested as a result of the π - π interaction between their aromatic ring moieties [26]. As more adsorbed salicylic acid can be the carbon source in following calcination process, thick carbon overlayer is hence observed in the TEM image (Fig. S2). Similar pattern is observed in ascorbic acid adsorption (high adsorption is accompanied with thick carbon overlayer), suggesting that in addition to the π - π interaction the hydrophobic interactions such as hydrophobic attraction between alkyl groups is

important in regulating the thickness of carbon overlayer (Fig. 2d). Importantly, as adsorbed organic acids are in principle functioning as the precursor of carbon source, the photocatalytic performance of as-obtained hematite electrodes is therefore more sensitive to the thickness of carbon overlayer rather than to the species of organic acid (Fig. 2a). Accordingly, the photocurrent of different hematite electrodes is closely related to the electrodeposition pH (Fig. 1a) as the latter regulates the thickness of carbon overlayer (Fig. 2a).

Aside from the adsorption behaviors, it is believed that an oxygen deficient environment, analog to coking processing [27] and steel manufacturing [28], is crucial in the formation of carbon overlayer. In fact, no carbon overlayer was found in the control experiments where organic acid adsorbed FeOOH particles were collected in the end of adsorption experiments and subjected to the identical two-stage calcinations. This substantially supports our above interpretation that surface adsorbed organic acids retaining in the voids of stacked FeOOH nanoparticles would have less access to ambient oxygen and therefore become the source of carbon overlayers (Fig. 4a). Interestingly, Fig. S2 shows that carbon overlayers are generally amorphous (without any significant fringes in TEM images) but occasionally crystallized carbon overlayers can be found as indicated in Fig. 4c. Occurrence of crystallized carbon overlayer implicates graphitization would also take place in the following calcination process. It has been reported that calcination of Fe(III) adsorbed sawdust in an oxygen deficient environment will produce intertwined graphitic tubules through catalytic graphitization [29]. The degree of graphitization was suggested closely related to the amount of Fe(III) adsorbed on saw dust but apparently it is not the case in this study as all calcinations were conducted in the confined voids resulting from the stacked FeOOH particles. In the contrary, the oxygen deficient environment seems to be the crucial factor controlling the crystallinity of carbon overlayer. Based on this consideration, it is realized that electrically reduced FeOOH nanoparticles are loosely stacked, which is consistent with observations in SEM images (Fig. S6). Occasionally, dead pores of stacked FeOOH particles occur and adsorbed organic acids happening to be retained in them therefore have opportunity to be graphitized carbon overlayer.

Fig. S6 exhibits the surface morphology of as-obtained hematite electrodes, which is significantly affected by the electrodeposition pH and the species of organic acid. Interestingly, changes in surface morphology (Fig. S6) should have significant influence on the photocatalytic performance of hematite [2,3] but observed volcano shaped correlation between the thickness of carbon overlayer and photocurrent suggested it is not the case (Fig. 2a). A rational explanation would be the fact that all electrically reduced FeOOH in this study are essentially three-dimensional structured particles. As a matter of fact, morphology-induced photocurrent enhancement is a result of the anisotropic conductivity of hematite where the conductivity within the (001) plane is 4 orders of magnitude higher than parallel to [001] [30]. In a three-dimensional structured particle, by contrast, the development of (001) plane is not significant over others. This speculation is supported by additional XRD analyses (Fig. 4d) where the (111) diffraction is much intense than any other planes in the region of 20–40 2-theta degree. Although the morphology effect on photocurrent enhancement is not significant in this study, it is obvious that adsorbed organic acids indeed lead the development of hematite particles to distinct morphology. A recent in situ ATR-FTIR analysis suggested that most organic acids will possess an outer-sphere configuration with the mineral surfaces in aqueous environments but gradually transform to an inner-sphere complexation under dry conditions [31]. We speculate this inner-sphere complexation configuration is responsible for different morphologies of carbon overlayer (Fig. S6). In fact, the affinity of organic acid to specific facet is important in directing the

morphology of hematite. For example, decreasing ethylene glycol content in a hydrothermal reaction was noted to retard the growth of (001) facet [32]. This is realized as the fact that (001) facet contains more relatively positive charged Fe(III) (in respect to oxygen) than any other facets based on crystallography consideration. As a result, morphology evolution from 2D structure (plates) to 1D structure (spindles) hematite is achieved when (001) facet is fully occupied by adsorbed organic acids [33]. Based on these considerations, an appropriate interpretation would be that the morphology effect is not significant enough to affect the photocatalytic performance of hematite. This is because the kinetic of charge transport in hematite electrolyte interface has been indicated the bottleneck in the enhancement of oxygen evolution reaction when the morphology of hematite electrodes are similar [33,34]. Nonetheless, it is certain that carbon overlayer significantly enhances the photocatalytic reactivity of hematite electrodes and an oxygen deficient environment resulting from the stacked FeOOH particles is crucial in converting adsorbed organic acid to carbon overlayer.

4. Conclusion

Our results suggest that it may be a universal case that hematite electrodes prepared by electrodeposition in the presence of organic acid additives can induce carbon overlayers. Furthermore, the capability to passivate surface states and to introduce additional charge carriers that reduce the onset photocurrent potential and enhance photocurrent plateau are the major attributes of carbon overlayers. Carbon overlayers also improved the photocurrent density to sustain for over 1000 s. Enhancement in durability of carbon overlayers and the correlation between the affinity of organic acid toward iron oxyhydroxides and subsequent PEC performance would be important research topics to understanding the functionality of carbon overlayers.

Acknowledgment

The authors wish to thank the Ministry of Science and Technology, Taiwan, for the support of this study by research grants: MOST 105-2113-M-007-022-MY2 and MOST 105-2119-M-007-013.

Appendix A. Supplementary data

Supplementary data associated with this article can be found, in the online version, at <http://dx.doi.org/10.1016/j.apcatb.2017.02.003>.

References

- [1] O. Zandi, T.W. Hamann, The potential versus current state of water splitting with hematite, *Phys. Chem. Chem. Phys.* 17 (35) (2015) 22485–22503.
- [2] D. Kang, T.W. Kim, S. Kubota, A. Cardiel, H.G. Cha, K.-S. Choi, Electrochemical synthesis of photoelectrodes and catalysts for use in solar water splitting, *Chem. Rev.* 115 (23) (2015) 12839–12887.
- [3] P.S. Shinde, A. Annamalai, J.Y. Kim, S.H. Choi, J.S. Lee, J.S. Jang, Fine-tuning pulse reverse electrodeposition for enhanced photoelectrochemical water oxidation performance of α -Fe₂O₃ photoanodes, *J. Phys. Chem. C* 119 (10) (2015) 5281–5292.
- [4] Q.Y. Zeng, J. Bai, J.H. Li, L.G. Xia, K. Huang, X.J. Li, B.X. Zhou, A novel in situ preparation method for nanostructured alpha-Fe₂O₃ films from electrodeposited Fe films for efficient photoelectrocatalytic water splitting and the degradation of organic pollutants, *J. Mater. Chem. A* 3 (8) (2015) 4345–4353.
- [5] O. Zandi, A.R. Schon, H. Hajibabaei, T.W. Hamann, Enhanced charge separation and collection in high-performance electrodeposited hematite films, *Chem. Mater.* 28 (3) (2016) 765–771.
- [6] J.Y. Zheng, S.I. Son, T. Khue Van, Y.S. Kang, Preparation of α -Fe₂O₃ films by electrodeposition and photodeposition of Co-Pt on them to enhance their photoelectrochemical properties, *RSC Adv.* 5 (46) (2015) 36307–36314.
- [7] W.D. Chemelewski, J.R. Rosenstock, C.B. Mullins, Electrodeposition of Ni-doped FeOOH oxygen evolution reaction catalyst for photoelectrochemical water splitting, *J. Mater. Chem. A* 2 (36) (2014) 14957–14962.

[8] F. Le Formal, N. Tétreault, M. Cornuz, T. Moehl, M. Grätzel, K. Sivula, Passivating surface states on water splitting hematite photoanodes with alumina overlayers, *Chem. Sci.* 2 (4) (2011) 737–743.

[9] M.G. Ahmed, I.E. Kretschmer, T.A. Kandiel, A.Y. Ahmed, F.A. Rashwan, D.F. Bahnemann, A facile surface passivation of hematite photoanodes with TiO_2 overlayers for efficient solar water splitting, *ACS Appl. Mater. Interfaces* 7 (43) (2015) 24053–24062.

[10] J.J. Deng, X.X. Lv, J. Gao, A.W. Pu, M. Li, X.H. Sun, J. Zhong, Facile synthesis of carbon-coated hematite nanostructures for solar water splitting, *Energy Environ. Sci.* 6 (2013) 1965–1970.

[11] T.H. Wang, Y.N. Chen, C.C. Chiang, Y.K. Hsieh, P.C. Li, C.F. Wang, Induced carbon layer on the surface of hematite electrodes with enhanced photoelectrochemical performance via the simple electrodeposition method with citric acid additive, *ChemElectroChem* 3 (6) (2016) 966–975.

[12] W.D. Schecher, D.C. McAvoy, MINEQL+: A Chemical Equilibrium Modeling System, Version 4.5 for Windows, User's Manual, v2.00, Environmental Research Software, Hallowell, Maine, 2003.

[13] J. Chatlas, R.B. Jordan, Complexation of the aqua-Iron(III) dimer by tiron – kinetics of complex-formation and dissociation, *Inorg. Chem.* 33 (17) (1994) 3817–3822.

[14] NIST X-ray Photoelectron Spectroscopy Database, NIST Standard Reference Database 20, Version 4.1, <http://srdata.nist.gov/xps/>.

[15] O. Zandi, T.W. Hamann, Enhanced water splitting efficiency through selective surface state removal, *J. Phys. Chem. Lett.* 5 (9) (2014) 1522–1526.

[16] B. Klahr, S. Gimenez, F. Fabregat-Santiago, J. Bisquert, T.W. Hamann, Electrochemical and photoelectrochemical investigation of water oxidation with hematite electrodes, *Energy Environ. Sci.* 5 (6) (2012) 7626–7636.

[17] C.X. Kronawitter, I. Zegkinoglou, C. Rogero, J.H. Guo, S.S. Mao, F.J. Himpel, L. Vayssières, On the interfacial electronic structure origin of efficiency enhancement in hematite photoanodes, *J. Phys. Chem. C* 116 (43) (2012) 22780–22785.

[18] Q. Yu, X.G. Meng, T. Wang, P. Li, J.H. Ye, Hematite films decorated with nanostructured ferric oxyhydroxide as photoanodes for efficient and stable photoelectrochemical water splitting, *Adv. Funct. Mater.* 25 (18) (2015) 2686–2692.

[19] L. Steier, I. Herraiz-Cardona, S. Gimenez, F. Fabregat-Santiago, J. Bisquert, S.D. Tilley, M. Grätzel, Understanding the role of underlayers and overlayers in thin film hematite photoanodes, *Adv. Funct. Mater.* 24 (48) (2014) 7681–7688.

[20] C. Du, X.G. Yang, M.T. Mayer, H. Hoyt, J. Xie, G. McMahon, G. Bischoping, D.W. Wang, Hematite-based water splitting with low turn-on voltages, *Angew. Chem. Int. Ed.* 52 (48) (2013) 12692–12695.

[21] C. Costentin, T.R. Porter, J.-M. Saveant, Conduction and reactivity in heterogeneous-molecular catalysis: new insights in water oxidation catalysis by phosphate cobalt oxide films, *J. Am. Chem. Soc.* 138 (17) (2016) 5615–5622.

[22] M.T. Mayer, Y.J. Lin, G.B. Yuan, D.W. Wang, Forming heterojunctions at the nanoscale for improved photoelectrochemical water splitting by semiconductor materials: case studies on hematite, *Accounts Chem. Res.* 46 (7) (2013) 1558–1566.

[23] H. Xia, C.Y. Hong, B. Li, B. Zhao, Z.X. Lin, M.B. Zheng, S.V. Savilov, S.M. Aldoshin, Facile synthesis of hematite quantum-dot/functionalized graphene-sheet composites as advanced anode materials for asymmetric supercapacitors, *Adv. Funct. Mater.* 25 (4) (2015) 627–635.

[24] T. Hisatomi, F. Le Formal, M. Cornuz, J. Brillet, N. Tétreault, K. Sivula, M. Grätzel, Cathodic shift in onset potential of solar oxygen evolution on hematite by 13-group oxide overlayers, *Energy Environ. Sci.* 4 (7) (2011) 2512–2515.

[25] P. Atkins, J. de Paula, *Physical Chemistry*, 8th edition, University Press, Oxford, 2006.

[26] R. Neubauer, M. Husmann, C. Weinlaender, N. Kienzl, E. Leitner, C. Hochenauer, Acid base interaction and its influence on the adsorption kinetics and selectivity order of aromatic sulfur heterocycles adsorbing on $Ag-Al_2O_3$, *Chem. Eng. J.* 309 (2017) 840–849.

[27] G.C. Abreu, J.A. de Carvalho, B.E. Correa da Silva, R.H. Pedrini, Operational and environmental assessment on the use of charcoal in iron ore sinter production, *J. Cleaner Prod.* 101 (2015) 387–394.

[28] L.D. Virla, V. Montes, J.F. Wu, S.F. Ketep, J.M. Hill, Synthesis of porous carbon from petroleum coke using steam, potassium and sodium: combining treatments to create mesoporosity, *Microporous Mesoporous Mat.* 234 (2016) 239–247.

[29] E. Thompson, A.E. Danks, L. Bourgeois, Z. Schnepp, Iron-catalyzed graphitization of biomass, *Green Chem.* 17 (2015) 551–556.

[30] A. Kleinan-Shwarzstein, Y.-S. Hu, A.J. Forman, G.D. Stucky, E.W. McFarland, Electrodeposition of α -Fe₂O₃ doped with Mo or Cr as photoanodes for photocatalytic water splitting, *J. Phys. Chem. C* 112 (2008) 15900–15907.

[31] S.H. Kang, B.S. Xing, Adsorption of dicarboxylic acids by clay minerals as examined by in situ ATR-FTIR and ex situ DRIFT, *Langmuir* 3 (13) (2007) 7024–7031.

[32] J. Zhao, P. Yang, H.S. Chen, J. Li, Q.D. Che, Y.N. Zhu, R.X. Shi, Effect of sequential morphology adjustment of hematite nanoplates to nanospindles on their properties and applications, *J. Mater. Chem. C* 3 (11) (2015) 2539–2547.

[33] C.G. Morales-Guio, L. Liardet, X. Hu, Oxidatively electrodeposited thin-film transition metal (Oxy)hydroxides as oxygen evolution catalysts, *J. Am. Chem. Soc.* 138 (28) (2016) 8946–8957.

[34] F. Le Formal, E. Pastor, S.D. Tilley, C.A. Mesa, S.R. Pendlebury, M. Grätzel, J.R. Durrant, Rate law analysis of water oxidation on a hematite surface, *J. Am. Chem. Soc.* 137 (20) (2015) 6629–6637.